Volume 1 | Number 1 | Jan 2013 | Pages 1–100

Journal of
Materials Chemistry A

Materials for energy and sustainability
www.rsc.org/materialsA

Li⁺

ROYAL SOCIETY
OF CHEMISTRY

ROYAL SOCIETY
OF CHEMISTRY

www.rsc.org/materialsA

Journal Name

ARTICLE

Efficient Ag_8GeS_6 Counter Electrode Prepared From Nanocrystal Ink for Dye-Sensitized Solar Cells

Qingquan He,[a] Tianyue Qian,[a] Jiantao Zai,*[a] Qiquan Qiao,[b] Shoushuang Huang,[a] Yiran Li[c] and Min Wang[a]

Ternary metal sulfides could provide more alternatives and tune physicochemical properties due to the presence of two cations. However, only Co/Ni-based ternary sulfides have been explored as counter electrode (CE) materials in dye-sensitized solar cells (DSSCs). Herein, CEs fabricated by Ag_8GeS_6 nanocrystal ink exhibited efficient electrocatalytic activity in the reduction of I_3^- to I^- in DSSCs. The DSSC with Ag_8GeS_6 CE displayed a higher power conversion efficiency of 8.10% than that with Pt CE (8.02%). Moreover, the devices also showed the characteristics of fast activity onset, high multiple start/stop capability and good irradiated stability. The results indicated that the developed Ag_8GeS_6 CE could be a promising alternative to Pt CE in DSSCs.

Introduction

Dye-sensitized solar cells (DSSCs) have recently attracted great attention owing to their easy fabrication and cost-effectiveness.[1, 2] As a crucial component, counter electrode (CE) plays an important role in the performance of DSSCs, which collects electrons from external circuit and fulfills electron transfer from CE to electrolyte by catalyzing the reduction of I_3^- to I^-. Ideally, CE materials should possess low resistance, high electrocatalytic activity and excellent chemical stability.[3, 4] Currently, platinum-loaded (Pt) conducting glass is widely exploited as a CE for DSSCs. However, Pt could dissolve in the electrolyte and create by-products because of the corrosive I^-/I_3^- redox electrolyte, such as PtI_4 and H_2PtI_6,[5, 6] which would deteriorate the long term stability of DSSCs. Therefore, tremendous research focus on the development of efficient and stable alternatives to Pt.[7-16] Binary transition metal sulfides were widely studied since CoS was first developed as CE material in DSSCs, due to its foreseeable electrocatalytic ability toward I_3^- reduction.[4, 6, 17-21] However, further development of CE materials for DSSCs is limited by the small number of suitable binary sulfides available. On the other hand, ternary metal sulfides would provide more alternatives and tune physicochemical properties due to the existence of two cations.[22] Up to now, only Co/Ni-based

ternary sulfides have been explored as CEs materials in DSSCs.[22-25]

Recently, Ag_8SnS_6 CE was fabricated for DSSCs by our group,[26] and showed the impressive electrocatalytic activity and stability in catalyzing I_3^- reduction. However, the photovoltaic performance of DSSCs based on Ag_8SnS_6 CE was still poor compared with that with Pt CE. Cartledge et al. considered that the higher ionic potential could cause higher polarizability,[27-29] which could promote the adsorption of I_3^- on CE materials and enhance the electrocatalytic efficiency of CE in DSSCs. So Ag_8GeS_6 would be a potential CE material due to its higher ionic potential (effective static potential of the cation) of Ge^{4+} compared with Sn^{4+}. Recently, Zhang et al. were first report the colloidal process to synthesize Ag_8GeS_6 nanocrystals using GeI_4 as Ge precursor.[30] Herein, Ag_8GeS_6 nanocrystal ink was prepared in a mixture of oleylamine (OAm) and 1-octadecene (ODE) with $AgNO_3$, $GeCl_4$ and sulfur as precursors, and used to fabricate CE for DSSCs for the first time. It is noteworthy that the DSSC with Ag_8GeS_6 CE displayed a power conversion efficiency of 8.10%, superior to that with Pt CE (8.02%).

Results and discussion

Typical XRD patterns (Fig. 1) indicate that the obtained products are of argyrodite Ag_8GeS_6 (JCPDS No. 83-1427). TEM image shows the as-prepared Ag_8GeS_6 is of monodispersed nanocrystals with the size about 7.5 nm (Fig. 2a and S1, see Supporting Information). HRTEM image reveals that the obtained nanocrystals are highly crystalline, and the interplanar distance of 0.305 nm corresponds to the (022) plane of argyrodite Ag_8GeS_6 (Fig. 2b). Moreover, the as-synthesized Ag_8GeS_6 nanocrystals can be easily dispersed into

[a.] Shanghai Electrochemical Energy Devices Research Center, School of Chemistry and Chemical Engineering and State Key Laboratory of Metal Matrix Composites, Shanghai Jiao Tong University, Shanghai, 200240, P. R. China
[b.] Center for Advanced Photovoltaics, South Dakota State University, Brookings, SD 57007, USA
[c.] Department of Materials Science and Engineering, Northwestern University, Evanston, IL 60201, USA

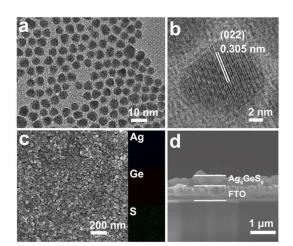**Fig. 1** Typical XRD patterns with the standard Ag_8GeS_6 (JCPDS No. 83-1427, red bar).

Fig. 2 (a, b) TEM and HRTEM images of Ag_8GeS_6 nanocrystals. (c, d) Top and cross-sectional SEM images of the densely packed Ag_8GeS_6 thin film on FTO glass, inset: the corresponding elemental mapping images.

chloroform to form a stable ink, which can be stable for at least one month (Fig. S2).

In order to investigate the formation mechanism of Ag_8GeS_6 nanocrystals, the products prepared at different stage were collected and characterized by XRD (Fig. S3). When the mixture of $AgNO_3$, $GeCl_4$, OAm and ODE was vigorously stirred and degassed by pulling vacuum in a flask, the chlorargyrite AgCl was formed. The color of solution turned from white to black after the injection of sulfur precursor, corresponding to the formation of acanthite Ag_2S. When the temperature was increased to 140 ^{o}C, the mixture of Ag_2S and Ag_8GeS_6 was obtained, which was inferred from the (022) peak of canfieldite Ag_8GeS_6. Further increasing the reaction temperature from 140 to 190 ^{o}C, the main peak ((−121) peak) of Ag_2S was getting weaker, and the main peak ((022) peak) of Ag_8GeS_6 was gradually becoming stronger, which means the

formation of Ag_8GeS_6 as the disappearance of Ag_2S. Based on the above experimental results, the formation of Ag_8GeS_6 nanocrystals can be proposed. The AgCl nanoparticles were formed in the mixed solution, and Ag_2S formed immediately once the sulfur precursor was injected. With the increase of reaction temperature, the Ge^{4+} progressively exchanged with Ag^+ in Ag_2S and finally evolved into Ag_8GeS_6 nanocrystals at about 190 ^{o}C. Thus the formation of Ag_8GeS_6

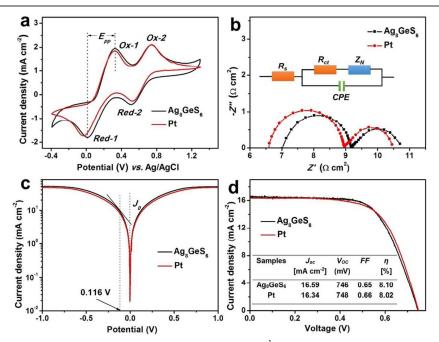**Fig. 3** (a) Cyclic voltammograms of Ag_8GeS_6 and Pt CEs measured at a scan rate of 50 mV s^{-1}. (b) Nyquist plots of the symmetrical cells based on different CEs. Inset: the equivalent circuit model. (c) Tafel polarization curves at the scan rate of 50 mV s^{-1} based on the same devices as in (b). (d) Current density-voltage characteristics of DSSCs based on different CEs measured under 100 mW cm^{-2}.

nanocrystal is mainly attributed to cation-exchange reactions that occur in silver-based chalcogenides, in which Ag^+ in ionic materials with high-density cation vacancies in the rigid sublattice of S^{2-} behaves like a "fluid" because of their high cationic mobility in vacancies.[31-35]

To fabricate Ag_8GeS_6 CE (Fig. S4), Ag_8GeS_6 nanocrystal ink with different concentrations (typical: 50 mg mL^{-1}) was spin-coated onto an FTO glass substrate at 800 rpm for 0.5 minute. The top and cross-sectional SEM images show that the Ag_8GeS_6 thin film is densely packed with thickness about 0.42 μm (Fig. 2c-d). The corresponding elemental mapping images of the film reveal the homogeneous distributions of Ag , Ge and S elements.

CV was used to scrutinize the electrocatalytic activity of Ag_8GeS_6 electrode towards the I^-/I_3^- redox couple. For comparison, Pt electrode was also studied under the same condition. Two pairs of redox peaks are observed on both electrodes (Fig. 3a), the left pair (*OX-1/Red-1*) and the right pair (*Ox-2/Red-2*), which correspond to the redox reactions of I^-/I_3^- ($I_3^- + 2\ e^- \rightarrow 3I^-$) and I_2/I_3^- ($3\ I_2 + 2\ e^- \rightarrow 2I_3^-$), respectively.[9, 36] As mentioned before, the CE in a DSSC serves to catalyze the reduction of I_3^-, thus the characteristics of the left pair are of research interest. The cathodic peak current density (J_{Red}) and peak-to-peak (E_{pp}) separation between anodic and cathodic peaks are important parameters for the electrocatalytic activity of CEs.[9, 19, 37] The higher $|J_{Red-1}|$ (1.81 mA cm^{-2}) and lower E_{pp} (0.31 V) suggest that Ag_8GeS_6 CE possesses better electrocatalytic activity than that of Pt CE (1.75 mA cm^{-2} and 0.35 V, respectively).

On the basis of promising CV results, the intrinsic interfacial charge transfer and charge transport kinetics at the electrode/electrolyte interface of CE in DSSCs can be conveniently evaluated by EIS.[19, 38] The EIS measurements were carried out with symmetrical cells fabricated with two identical electrodes. The Nyquist plots were fitted with an equivalent circuit model with Z-view software (Fig. 3b and S5) and the corresponding photovoltaic parameters are summarized in Table 1 and S1. The charge transfer resistance at the electrolyte/electrode interface (R_{ct}) was obtained by fitting the semicircle in the high-frequency region (left semicircle), while the right semicircle in the low-frequency range indicates the Nernst diffusion impedance (Z_N) of the I_3^-/I^- redox couple in electrolyte.[7, 39] The smaller R_{ct} of the Ag_8GeS_6 CE indicates its higher electrocatalytic activity for the reduction of I_3^- in DSSCs,[19, 37] which could promote the dye regeneration on photoanode and further improve the photocurrent density of DSSCs.[37] These results can also be confirmed by Tafel polarization curves (Fig. 3c). The greater slope of the *J-V* plot in Tafel curves indicates higher exchange current density (J_0) of Ag_8GeS_6 CE than that of Pt CE.[4, 19] However, the corresponding constant phase-angle element (CPE) value for the Ag_8GeS_6 CE is 10.02 μF, which is lower than that of the Pt CE with a CPE value of 10.41 μF. The fact may be presumably due to the smaller particles of Pt, resulting in the larger surface roughness of Pt CE.[40]

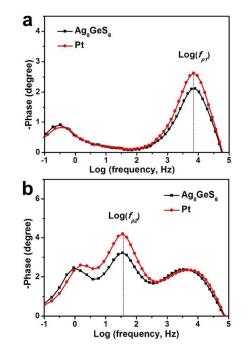Taking the results of CV, EIS and Tafel polarization into consideration, Ag_8GeS_6 CEs displayed higher electrocatalytic

Fig. 4 Bode phase plots of (a) symmetric dummy cells and (b) DSSCs with Ag_8GeS_6 and Pt CEs.

activity towards the reduction of I_3^- compared with Pt CEs, making them potentially good performance for constructing DSSCs. To further assess the above results, DSSCs were fabricated using Ag_8GeS_6 and Pt CEs. The photovoltaic performances of the DSSCs with various CEs are shown in Fig. 3d, and the corresponding parameters are summarized in the inset. As shown in Fig. 3d, the short-circuit photocurrent density (J_{sc}), open-circuit voltage (V_{oc}) and fill factor (*FF*) of DSSCs with Ag_8GeS_6 CE are 16.59 mA cm^{-2}, 746 mV and 0.65, respectively, yielding an overall energy-conversion efficiency (*η*) of 8.10%.

Meanwhile, the DSSC with Pt exhibits a J_{sc} of 16.34 mA cm^{-2}, a V_{oc} of 748 mV, a *FF* of 0.66, and a *η* of 8.02%. These results demonstrate that Ag_8GeS_6 CE possesses better performance in DSSCs than Pt. This can be further supported by the incident photon to charge carrier efficiency (IPCE) spectra (Fig. S8a). Futhermore, Ag_8GeS_6 CEs with different thicknesses were also assembled into DSSCs. The corresponding current density-voltage (*J-V*) curves are shown in Fig. S7, and the solar cell parameters are summarized in Table S4. The results indicate that the *η* of DSSCs can be improved by optimizing the thickness of Ag_8GeS_6 CEs.

Fig. 4a represents the Bode spectra of symmetric dummy cells with Ag_8GeS_6 and Pt CEs. The lifetime of electrons (τ_1) in the I_3^- reduction at the CE/electrolyte interface can be calculated according to $\tau_1 = 1/2\pi f_{p1}$,[41, 42] where f_{p1} is the peak of high-frequency region in the spectra (Table 1). The τ_1 value of DSSC with Ag_8GeS_6 CE (27.0 μs) is samller than that with Pt (28.3 μs), meaning higher electrocatalytic activity towards I_3^- reduction. Meanwhile, the photoelectron lifetime (τ_2) in the photoanode of the DSSC with Ag_8GeS_6 CE (4602.2 μs) is longer

Table 1. Photovoltaic parameters of DSSCs with different CEs and the simulated data from EIS spectra.

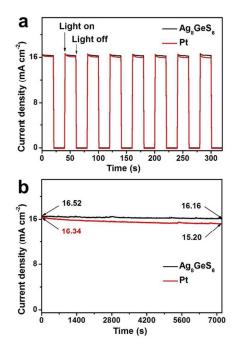| Samples	E_{pp} [V]	R_{ct} [Ω cm^2]	f_1 [Hz]	τ_1 [μs]	f_2 [Hz]	τ_2 [μs]
Ag$_8$GeS$_6$	0.32	2.16	5888.4	27.0	34.6	4602.2
Pt	0.35	2.38	5623.4	28.3	36.3	4386.7

Fig. 5 (a) Start-stop switches and (b) photocurrent stabilities of the DSSCs with Ag$_8$GeS$_6$ and Pt electrodes. The on-off plots were achieved by alternately irradiating (100 mW cm^{-2}) and darkening (0 mW cm^{-2}) the DSSC devices at 0 V, whereas the photocurrent stabilities were carried out under a sustained irradiation of 100 mW cm^{-2} at 0.45 V.

than that with Pt CE (4386.7 µs). The result implies that Ag$_8$GeS$_6$ CE can facilitate the flow of electrons from the excited dye to the conduction band of TiO$_2$, and can further reduce the recombination of photogenerated carriers in the photoanode (Fig. 4b).[41]

As a crucial component of DSSCs, CEs are required fast start-up and multiple start/stop cycling for their applications. An sudden increase in the photocurrent density at"light on" and no delay in starting the cells suggest the rapid response of Pt and Ag$_8$GeS$_6$ CEs for I$_3^-$ reduction (Fig. 5a).[41] The stability of the DSSCs under prolonged irradiation was evaluated by measuringthe device can be improved by employing Ag$_8$GeS$_6$ CE. the photovoltaic performance in sustained irradiation for 2 hours (Fig. 5b). Only 2.2% of the initial photocurrent density decreases for the DSSC with Ag$_8$GeS$_6$ CE compared with that with Pt CE (7.8%). Although the DSSCs were tested for only 2 hours, the preliminary result demonstrates that the stability of can be improved by employing Ag$_8$GeS$_6$ CE.
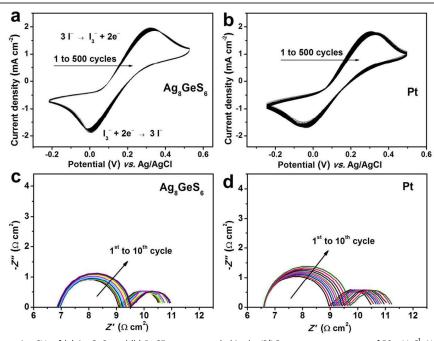

Fig. 6 A total of 500 consecutive CVs of (a) Ag$_8$GeS$_6$ and (b) Pt CEs were recorded in the I$^-$/I$_3^-$ system at a scan rate of 50 mV s^{-1}. Nyquist plots of EIS data for the symmetrical cells with (c) Ag$_8$GeS$_6$ and (d) Pt electrodes. The cells were first subjected to CV scanning from 0 to 1 V and then from −1 to 0 V with a scan rate of 100 mV s^{-1}, followed by 20 s relaxation at 0 V. EIS measurement at 0 V from 100 kHz to 100 mHz was then performed. This sequential electrochemical test was repeated 10 times.
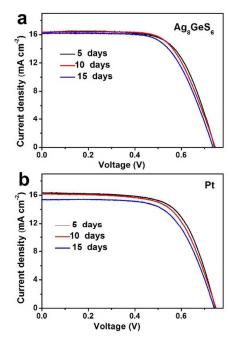
Fig. 7 *J–V* characteristics of DSSCs with Ag_8GeS_6 and Pt CEs, which were dipped in iodine electrolyte for different times.

Multiple CVs further reinforced, after 500 cycles, that the Ag_8GeS_6 CE was more stable than the Pt CE (Fig. 6a-b). Moreover, DSSCs with Ag_8GeS_6 and Pt CEs were assembled and continuously tested for fifteen days to investigate their long-term stability (Fig. S9-S10 and Table S5-S6). After 15 days, the J_{sc}, FF and η of DSSCs with the Ag_8GeS_6 CE retained 81.8%, 95.4% and 78.1% of their original value, while ones with Pt CE are of 69.7%, 92.4% and 65.4%, respectively. If the fabricated CEs were dipped in the iodine based electrolyte for 15 days (Fig. S11 and Table S7-S8) and then assembled into DSSCs, the retention rate of cells with Ag_8GeS_6 CE (95.6%) is higher than that of Pt CE (91.4%). The above results further emphasizing the high chemical stability of Ag_8GeS_6 CE in iodine based electrolytes. Additionally, the electrochemical stability of CEs was also examined through repeated EIS measurements of 10 cycles (Fig. 6c-d). Almost no changes in R_s and Z_N for all samples were found, meaning the potential cycling hardly influences the series resistance and the mass transport in the redox electrolyte solution.[19] However, R_{ct} value increased from 2.16 to 2.63 Ω cm^2 for Ag_8GeS_6 CE (21.7%) and from 2.38 to 3.12 Ω cm^2 for Pt CE (31.1%), which are consistent with the above results.

Conclusions

In summary, Ag_8GeS_6 nanocrystal ink was prepared *via* a colloidal synthesis process with simple inorganic compounds as precursors. The obtained nanocrystal ink was prepared into CEs for DSSCs. This newly developed Ag_8GeS_6 CE displayed lower charge transfer resistance, better chemical stability and higher catalytic activity toward I_3^- reduction compared with Pt

CE in DSSCs. Notably, the device consisting of Ag_8GeS_6 CE displayed a η of 8.10%, superior to that with Pt CE (8.02%).

Experimental section

Materials and reagents

Silver nitrate ($AgNO_3$, 99.9%, Shanghai Institute of Fine Chemical Materials), oleylamine (OAm, 70%, Sigma-Aldrich), 1-octadecene (ODE, 90%, Alfa Aesar) and sublimed sulfur (99.5%, Sinopharm Chemical Reagent Co., Ltd) were purchased and used as received without further purification. Transparent conductive glass (F-doped SnO_2, FTO, 15 Ω/square, transmittance of 80%) was purchased from Yingkou OPV Tech New Energy Co., Ltd.

Preparation of Ag_8GeS_6 nanocrystal ink

In a typical synthesis process, 2 mmol of $AgNO_3$ (0.340 g) and 0.25 mmol $GeCl_4$ (30 μL) were dissolved in a mixture of OAm (1.0 mL) and ODE (9.0 mL) by vigorously stirring and degassing in a three-neck flask at 60 ºC for 30 minutes. Then the above system was heated to 140 ºC in 20 minutes under a nitrogen atmosphere. After a mixture of sublimed sulfur (2.5 mmol) and OAm (2.5 mL) was immediately injected into the three-neck flask with a syringe, the reaction system was heated to 200 ºC at a rate of 4 ºC min^{-1} and maintained for 30 minutes. Then the flask was removed from the heating mantle and cooled to room temperature naturally. Finally, precipitates were collected after 30 mL of ethanol was added to the reactant solution, followed by centrifugation at 4000 rpm for 5 minutes. Then the precipitate was redispersed in chloroform. Prior to characterization, dispersions were typically centrifuged again at 8000 rpm for 5 minutes to remove inadequately capped particles.

Preparation of counter electrodes

CEs were prepared by spin-coating the solution of as-prepared products (SpinMaster 100, Chemat Technology, Inc.) onto a cleaned FTO glass substrate. The thicknesses of the CEs were controlled by the concentrations of as-synthesized nanocrystals in chloroform (10, 20, 50 and 120 mg L^{-1}). Then the coated substrates were placed on a hot plate (60 ^{o}C) for 10 minutes to evaporate the volatile solvent, and subsequently sintered at 400 ^{o}C for 30 minutes in nitrogen atmosphere (air for Pt CE). After being annealed, the films were slowly cooled to room temperature.

Fabrication of dye-sensitized solar cells

Photoanodes were purchased from Yingkou OPV Tech New Energy Co., Ltd. TiO_2 films (~ 15 μm in thickness) containing transparent (~ 11 μm) and scattering (~ 4 μm) layers with the apparent area of 0.16 cm^2. TiO_2 films were immersed into 5 mmol L^{-1} ethanol solution of ruthenium 535 bis-TBA (N719, Solaronix SA) for 24 hours. The dye-sensitized TiO_2 photoanode and the as-prepared CE were separated by a hot-melt Surlyn film (60 μm thick) and sealed by hot-pressing. The cell internal space was filled with electrolytes using a vacuum pump. The redox electrolyte composed of 0.03 mol L^{-1} of I_2, 0.6 mol L^{-1} of 1-butyl-3-methylimi-dazolium iodide, 0.5 mol L^{-1}

of 4-tert-butyl pyridine and 0.1 mol L^{-1} of guanidinium thiocyanate with anhydrous acetonitrile as solvent.[7] Finally, the holes on the back of CE were sealed with a Surlyn film covered with a thin glass slide under heat.

Characterizations

The phase of the as-prepared products was characterized on a powder XRD (Shimadzu XRD-6000) equipped with a Cu Kα radiation source (λ = 1.5418 Å) at a scanning rate of 6° min^{-1} (2ϑ from 20° to 60°). The morphology and crystal lattice of samples were characterized by high-resolution transmission electron microscopy (HRTEM, JEOL, JEM-2100). The top/cross-sectional morphologies and energy dispersive X-ray spectrum (EDX) of Ag_8GeS_6 CEs were examined by field emission scanning electronic microscopy (FESEM, FEI Nova NanoSEM NPE218).

Cyclic voltammetry (CV) was carried out in a three-electrode system containing an anhydrous acetonitrile solution of $LiClO_4$ (0.1 mol L^{-1}), LiI (10 mmol L^{-1}) and I_2 (1 mmol L^{-1}) at a scan rate of 50 mV s^{-1}. Pt worked as counter electrode, the as-prepared CE as work electrode and Ag/AgCl as reference electrode. For electrochemical impedance spectroscopy (EIS), the symmetrical dummy cells were assembled with two identical CEs filled with the same electrolyte (CE//electrolyte//CE) as used in the DSSCs. The active apparent area of the dummy cell was 0.36 cm^2. In EIS tests, the samples were scanned from 100 kHz to 100 mHz at 0 V bias and ac amplitude of 10 mV. The resultant impedance spectra were analyzed using the Z-view non-linear least-squares fitting program. Tafel polarization curves were recorded on the same workstation by assembling symmetric cells. The photocurrent density-voltage (J-V) curves of DSSCs were recorded under the illumination of AM 1.5G simulated solar light coming from a Oriel Sol 3A solar simulator (Newport-69920) equipped with a Xe lamp (450 W) and an AM 1.5G filter with the scan direction from the open-circuit to the short-circuit at a scan rate of 50 mV s^{-1}. The light intensity was calibrated using a reference Si solar cell (Oriel-91150). All the electrical data was recorded on an electrochemical workstation (Zahner Zennium CIMPS-1, Germany).

Acknowledgements

Notes and references

1. B. O'Regan and M. Gratzel, *Nature*, 1991, **353**, 737-740.
2. A. Yella, H.-W. Lee, H. N. Tsao, C. Yi, A. K. Chandiran, M. K. Nazeeruddin, E. W.-G. Diau, C.-Y. Yeh, S. M. Zakeeruddin and M. Grätzel, *Science*, 2011, **334**, 629-634.
3. Y. Xue, J. Liu, H. Chen, R. Wang, D. Li, J. Qu and L. Dai, *Angew. Chem. Int. Ed.*, 2012, **51**, 12124-12127.
4. M. Wang, A. M. Anghel, B. Marsan, N.-L. Cevey Ha, N. Pootrakulchote, S. M. Zakeeruddin and M. Grätzel, *J. Am. Chem. Soc.*, 2009, **131**, 15976-15977.
5. E. Olsen, G. Hagen and S. Eric Lindquist, *Sol Energ Mat Sol C*, 2000, **63**, 267-273.
6. S. Huang, Q. He, W. Chen, J. Zai, Q. Qiao and X. Qian, *Nano Energy*, 2015, **15**, 205-215.
7. Y. Hou, D. Wang, X. H. Yang, W. Q. Fang, B. Zhang, H. F. Wang, G. Z. Lu, P. Hu, H. J. Zhao and H. G. Yang, *Nat. Commun.*, 2013, **4**, 1583.
8. S.-J. Yuan, Z.-J. Zhou, Z.-L. Hou, W.-H. Zhou, R.-Y. Yao, Y. Zhao and S.-X. Wu, *Chem. Eur. J.*, 2013, **19**, 10107-10110.
9. Z. Yang, M. Liu, C. Zhang, W. W. Tjiu, T. Liu and H. Peng, *Angew. Chem. Int. Ed.*, 2013, **52**, 3996-3999.
10. S. Das, P. Sudhagar, V. Verma, D. Song, E. Ito, S. Y. Lee, Y. S. Kang and W. Choi, *Adv. Funct. Mater.*, 2011, **21**, 3729-3736.
11. S. Sigdel, A. Dubey, H. Elbohy, A. Aboagye, D. Galipeau, L. F. Zhang, H. Fong and Q. Q. Qiao, *J. Mater. Chem. A*, 2014, **2**, 11448-11453.
12. P. Joshi, L. F. Zhang, Q. L. Chen, D. Galipeau, H. Fong and Q. Q. Qiao, *ACS Appl. Mater. Interfaces*, 2010, **2**, 3572-3577.
13. Y. Peng, J. Zhong, K. Wang, B. F. Xue and Y. B. Cheng, *Nano Energy*, 2013, **2**, 235-240.
14. T. H. Lee, K. Do, Y. W. Lee, S. S. Jeon, C. Kim, J. Ko and S. S. Im, *J. Mater. Chem.*, 2012, **22**, 21624-21629.
15. L. Cheng, Y. Hou, B. Zhang, S. Yang, J. W. Guo, L. Wu and H. G. Yang, *Chem. Commun.*, 2013, **49**, 5945-5947.
16. D. H. Youn, M. Seol, J. Y. Kim, J.-W. Jang, Y. Choi, K. Yong and J. S. Lee, *ChemSusChem*, 2013, **6**, 261-267.
17. Y. F. Du, J. Q. Fan, W. H. Zhou, Z. J. Zhou, J. Jiao and S. X. Wu, *ACS Appl. Mater. Interfaces*, 2012, **4**, 1796-1802.
18. S. Huang, Q. He, J. Zai, M. Wang, X. Li, B. Li and X. Qian, *Chem. Commun.*, 2015, **51**, 8950-8953.
19. F. Gong, H. Wang, X. Xu, G. Zhou and Z.-S. Wang, *J. Am. Chem. Soc.*, 2012, **134**, 10953-10958.
20. C. Chen, M. D. Ye, N. Zhang, X. R. Wen, D. J. Zheng and C. J. Lin, *J. Mater. Chem. A*, 2015, **3**, 6311-6314.
21. J. Song, G. R. Li, G. Xi, B. Lei, X. P. Gao and R. V. Kumar, *J. Mater. Chem. A*, 2014, **2**, 10041-10047.
22. Z. Shi, K. Deng and L. Li, *Sci. Rep.*, 2015, **5**, 9317.
23. J. Y. Lin and S. W. Chou, *Electrochem. Commun.*, 2013, **37**, 11-14.
24. A. Banerjee, K. K. Upadhyay, S. Bhatnagar, M. Tathavadekar, U. Bansode, S. Agarkar and S. B. Ogale, *RSC Adv.*, 2014, **4**, 8289-8294.
25. X. Zheng, J. Guo, Y. Shi, F. Xiong, W.-H. Zhang, T. Ma and C. Li, *Chem. Commun.*, 2013, **49**, 9645-9647.
26. Q. He, S. Huang, C. Wang, Q. Qiao, N. Liang, M. Xu, W. Chen, J. Zai and X. Qian, *ChemSusChem*, 2015, **8**, 817-820.
27. J. B. Umland and J. M. Bellama, *General chemistry*, Brooks/Cole Publishing Company, 1999.
28. P. A. Cox, *Instant notes inorganic chemistry*, Science Press, 2000.
29. K. P. Jensen and W. L. Jorgensen, *J. Chem. Theory Comput.*, 2006, **2**, 1499-1509.
30. B. Zhou, Y. Xing, S. Miao, M. Li, W.-H. Zhang and C. Li, *Chem. Eur. J.*, 2014, **20**, 12426-12431.
31. D. O. Demchenko, R. D. Robinson, B. Sadtler, C. K. Erdonmez, A. P. Alivisatos and L.-W. Wang, *ACS Nano*, 2008, **2**, 627-636.

32.   P.-J. Wu, J.-W. Yu, H.-J. Chao and J.-Y. Chang, *Chem. Mater.*, 2014, **26**, 3485-3494.

33.   Q. A. Akkerman, A. Genovese, C. George, M. Prato, I. Moreels, A. Casu, S. Marras, A. Curcio, A. Scarpellini, T. Pellegrino, L. Manna and V. Lesnyak, *ACS Nano*, 2015, **9**, 521-531.

34.   G. Krylova, L. J. Giovanetti, F. G. Requejo, N. M. Dimitrijevic, A. Prakapenka and E. V. Shevchenko, *J. Am. Chem. Soc.*, 2012, **134**, 4384-4392.

35.   J. Wang, K. Chen, M. Gong, B. Xu and Q. Yang, *Nano Lett.*, 2013, **13**, 3996-4000.

36.   M. Wu, X. Lin, A. Hagfeldt and T. Ma, *Angew. Chem. Int. Ed.*, 2011, **50**, 3520-3524.

37.   X. Zheng, J. Deng, N. Wang, D. Deng, W.-H. Zhang, X. Bao and C. Li, *Angew. Chem. Int. Ed.*, 2014, **53**, 7023-7027.

38.   S. H. Chang, M. D. Lu, Y. L. Tung and H. Y. Tuan, *ACS Nano*, 2013, **7**, 9443-9451.

39.   M. Wu, X. Lin, T. Wang, J. Qiu and T. Ma, *Energy Environ. Sci.*, 2011, **4**, 2308-2315.

40.   Y.-C. Wang, D.-Y. Wang, Y.-T. Jiang, H.-A. Chen, C.-C. Chen, K.-C. Ho, H.-L. Chou and C.-W. Chen, *Angew. Chem. Int. Ed.*, 2013, **52**, 6694-6698.

41.   X. Chen, Q. Tang, B. He, L. Lin and L. Yu, *Angew. Chem. Int. Ed.*, 2014, **53**, 10799-10803.

42.   J. Yoon, M. Jin and M. Lee, *Adv. Mater.*, 2011, **23**, 3974-3978.